COMPDYN 2011
III ECCOMAS Thematic Conference on
Computational Methods in Structural Dynamics and Earthquake Engineering
M. Papadrakakis, M. Fragiadakis, V. Plevris (eds.)
Corfu, Greece, 25–28 May 2011

ON THE SEISMIC BEHAVIOUR AND DESIGN OF LIQUID STORAGE TANKS

Patricia Pappa[1], Daniel Vasilikis[1], Polynikis Vazouras[2], and Spyros A. Karamanos[1]

[1] Department of Mechanical Engineering
University of Thessaly, Volos, Greece
e-mail: {davasili, patrpap, skara}@mie.uth.gr

[2] Department of Civil Engineering
University of Thessaly, Volos, Greece
e-mail: pvazour@yahoo.gr

Keywords: liquid storage tank, seismic design, sloshing, finite elements, shell buckling.

Abstract. *The paper examines some special issues on the structural behaviour of upright-cylindrical liquid storage tanks, which are widely used in industrial facilities and for water storage. Two main design standards are considered: EN 1998-4, a relatively new standard, and Appendix E of API 650, which has been through substantial amendments and revisions in its new version (11th edition, 2007). There are significant differences between the two specifications, which are due to the fact that there exist several controversial issues on this subject, open to further research. These issues are (a) the number of modes necessary to estimate accurately the convective seismic force due to the hydrodynamic behaviour of the liquid containment; (b) the appropriate combination of the impulsive and the convective component of seismic force; (c) the uplifting behaviour of unanchored tanks, with emphasis on the base plate behaviour and the increase of meridional compression; (d) the choice of an appropriate reduction (behaviour) factor for calculating both the impulsive and the convective force; (e) the calculation of hydrodynamic hoop stresses due to liquid hydrodynamic motion; (f) the design of tanks against buckling at the top due to liquid sloshing; (g) the importance of nonlinear wave sloshing effects.*

The present paper is aimed at addressing the above issues based mainly on numerical simulations. To simulate the tank shell and its structural behaviour, general-purpose finite element software ABAQUS is employed, whereas to examine hydrodynamic effects, an in-house numerical technique is developed. Existing data from previous investigations are also considered. The results are aimed at better understanding of liquid storage tank seismic behaviour, bridging the gap between the two major design standards (EN 1998-4 and API 650-Appendix E), towards safer seismic design of industrial facilities.

1 INTRODUCTION

The structural response of liquid storage tanks under strong seismic loading constitutes an important issue for safeguarding the structural integrity of industrial facilities, especially in refineries and power plants. Significant damages of tanks have been reported in earthquake events [1][2]. The dominant mode of tank failure is in the form of elephant's foot buckling at the tank base. Other types of earthquake damages include buckling of the top of the tank shell, base plate failure due to uplifting, roof damage due to excessive sloshing, or shell damage at nozzle areas due to non-flexible connections with piping. Current design practice is based on the application of the API 650 provisions [3], as described in Appendix E. This Appendix has been initially incorporated in the standard in the late 70's [4], and has been substantially revised in the 11th edition published in 2007 [3] to be in accordance with the provisions of ASCE 7-05 [5]. In addition, to this standard, the newly published EN 1998-4 standard [6] contains design provisions for the seismic design of liquid storage tanks.

In the following, several issues related to the seismic analysis of liquid storage tanks and the determination of seismic action are addressed and examined, using numerical simulations. It has been recognized that there exist some specific issues that require further investigation and improvement. In particular, the following issues are addressed in the present study:

- The number of sloshing modes to be considered in convective action and their combination with impulsive action.
- The effects of shell deformation on the seismic response.
- Calculations of hoop hydrodynamic stresses
- Uplifting of unanchored tanks
- Buckling at the top of the tank
- Behavior factor of liquid storage tank and elephant's foot buckling
- Nonlinear sloshing effects

The investigation of those issues is aimed at comparing – where possible – the API 650 and the EN 1998-4 provisions for the seismic design of liquid storage tanks, towards proposing possible improvements/amendments of the EN 1998-4 standard. For this purpose, three liquid storage tanks are considered and their seismic response is simulated numerically:

(a) A moderately-broad tank, referred to as Tank I, is primarily considered. This is a 27.4-meter-diameter tank with a total height of 16.5 meters. The tank is unanchored. The filling height of the tank H is equal to 15.7, which makes an aspect ratio of the tank $\gamma(H/R)$ equal to 1.145. The tank thickness varies from 6.4 mm at its top course to 17.7 mm at its bottom course, the bottom plate is 6 mm thick, and has a 8-mm-thick annular plate.

(b) The second tank considered, referred to as Tank II, is a tall tank of 18-meter-diameter tank with a total height of 20 meters. The filling height of the tank H is equal to 19, which makes an aspect ratio of the tank H/R equal to 2.1. The tank thickness varies from 6 mm at its top course to 10 mm at its bottom course and it is anchored .

(c) The third tank, referred to as Tank III, is a very broad tank of 68-meter-diameter with a total height of 20 meters. The filling height of the tank H is equal to 19 resulting to an aspect ratio H/R equal to 0.558. The tank thickness varies from 34 mm at its top course to 38.5 mm at its bottom course.

All three of the above liquid storage tanks are existing tanks, constructed in seismic regions, and have been designed against hydrostatic pressure following the API 650 [3] methodology "Calculation of Thickness by the 1-Foot Method" in section 5.6.3, considering a liquid containment of unit gravity (water). The tanks are depicted in Figure 1.

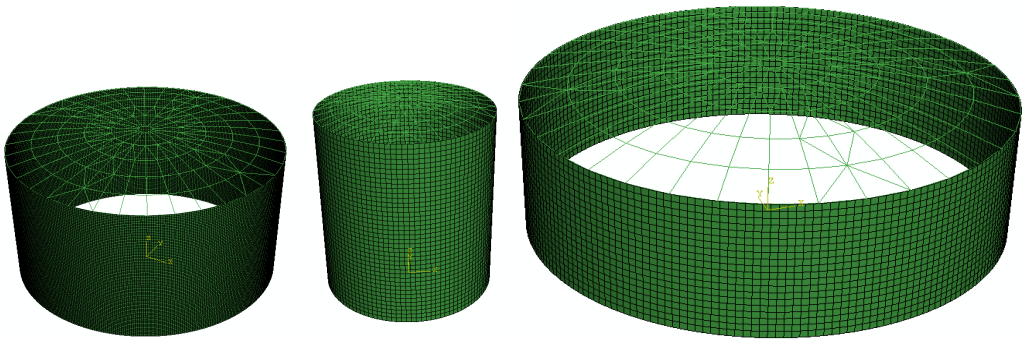

Figure 1: Tank I (left), tank II (center) and tank III (right) used for the parametric studies in the present paper.

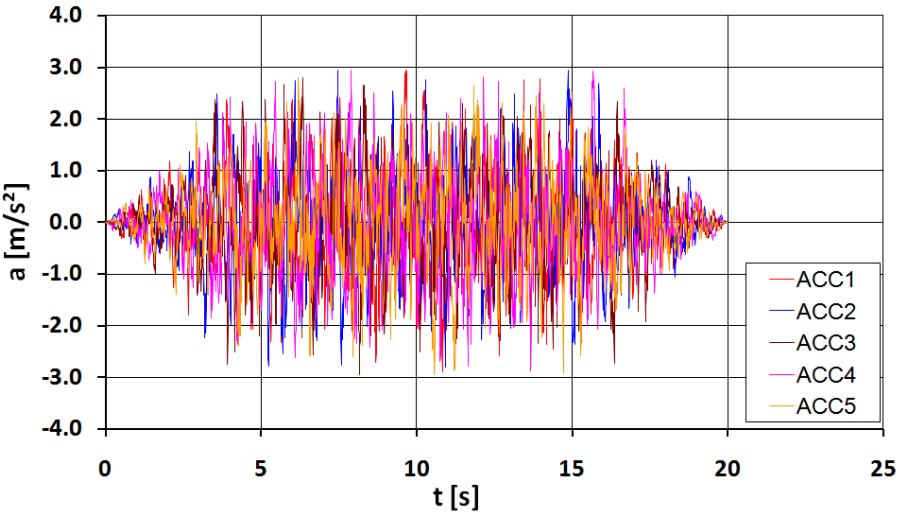

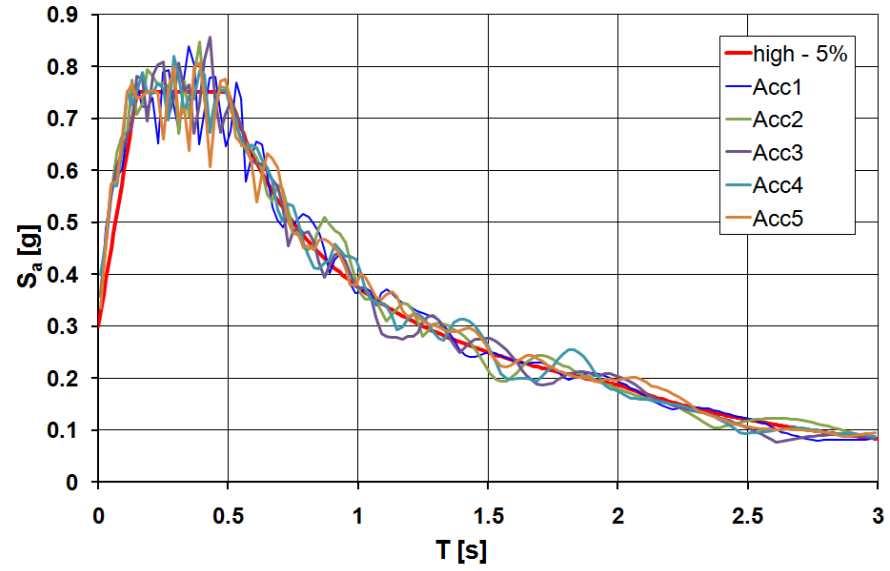

Figure 2: Artificial seismic accelerograms used in the present study (maximum ground acceleration is 0.25g) and their comparison with the 5% damping design spectrum of EN 1998-1.

2 SEISMIC DESIGN CODES FOR LIQUID STORAGE TANKS

Seismic design of liquid storage tanks in petrochemical facilities has been conducted with the relevant provisions of API 650. In particular, Appendix E of API 650 refers exclusively to seismic design, contains provisions for both determining seismic actions on tanks, as well as calculating the strength of the tank. The new edition of Appendix E includes provisions for site-specific seismic input, calculation of hoop hydrodynamic stresses, distinction between ringwall and slab overturning moments, freeboard requirements, and consideration of vertical excitation effects. The latter three issues are new, with respect to the old version of the Appendix [4], whereas the issues of uplifting/anchorage and calculation of shell compression are significantly enhanced. It should be noted that seismic action calculations in the new version of Appendix E are in accordance with ASCE 7 standard [5].

European standard EN 1998-4 [6] is part of the CEN/TC250 standards, often referred to as "Structural Eurocodes". It includes seismic provisions for silos, tanks and pipelines. In Chapter 2 some general provisions are stated. More specific rules for the seismic design of tanks are stated in Chapter 4 (e.g. behavior factor, limit state description), whereas extensive methodologies for calculating seismic action and verifying shell buckling are presented in Informative Annex A. It has been recognized as a standard that contains state-of-the-art scientific information for determining seismic action, based on the work of Rammerstorfer et al. [7] and Scharf [8] as well as the work of Rotter [9] for shell buckling under internal pressure (elephant's foot). However, there are some issues that need further investigation and possible improvement; a list of those issues is offered in section 1, and will be discussed extensively in the present paper.

3 SLOSHING MODES AND THEIR COMBINATION WITH IMPUSIVE MOTION

The first issue of interest concerns the number of sloshing (convective) modes to be considered for determining the convective seismic force. The three tanks under consideration have been subjected to base-ground seismic acceleration from 10 artificial earthquakes, generated from the EN 1998-1 design spectrum, as shown in Figure 2. Tables 1 and 2 show some characteristic results from 4 typical accelerograms from those earthquakes (denoted as ACC1, ACC2, ACC3 and ACC4 respectively), in terms of the maximum convective forces for several modes, the corresponding maximum impulsive force, and the maximum total seismic force. For each earthquake event the maximum convective force was calculated as the product of the "convective" accelerations and the corresponding sloshing masses:

$$F_C = \left(\sum_n \mathsf{M}_{nC}\ \ddot{u}_n \right)_{\max} \tag{1}$$

where the "convective" acceleration is calculated from the following linear oscillator equation:

$$\ddot{u}_n + 2\xi_n \omega_n \left(\dot{u}_n - \dot{X} \right) + \omega_n^2 \left(u_n - X \right) = 0 \tag{2}$$

In the above equations, the convective (sloshing) mass is computed as follows

$$\frac{\mathsf{M}_{nC}}{\mathsf{M}_L} = \frac{2 \tanh\left(k_n R\ \gamma\right)}{k_n R \gamma \left(k_n^2 R^2 - 1\right)} \tag{3}$$

and

$$\frac{\omega_n^2 R}{g} = \left(k_n R\right) \left[\tanh\left(k_n R\ \gamma\right) \right] \tag{4}$$

is the sloshing (convective) circular frequency of the tank. Similarly, the maximum impulsive force was calculated as the product of the "impulsive" acceleration and the corresponding impulsive mass:

$$F_I = \left(\mathbf{M}_I \ddot{X} \right)_{\max} \tag{5}$$

where the "impulsive" acceleration is calculated as follows

$$\ddot{u}_I + 2\xi_I \omega_I \left(\dot{u}_I - \dot{X} \right) + \omega_I^2 \left(u_I - X \right) = 0 \tag{6}$$

In the above equation, the impulsive mass is computed as follows

$$\mathbf{M}_I = \mathbf{M}_L - \sum_{n=1,2,3,\ldots} \mathbf{M}_{nC} \tag{7}$$

and

$$\omega_I = \frac{2\pi}{C_i} \sqrt{\frac{Et}{\rho R}} \tag{8}$$

is the impulsive circular frequency of the tank. In the above expression C_i is a nondimensional parameter that depends on the aspect ratio of the tank $\gamma = H/R$ and where t is the average thickness of the tank shell. The integration of linear oscillator equations (2) and (6) is performed through a standard central-difference numerical method. In Tables 1, 2, and in Figure 3a, Figure 3b and Figure 3c, together with the maximum convective and impulsive forces, the maximum total forces are presented, for 4 typical artificial ground acceleration inputs (denoted as ACC1, ACC2, ACC3 and ACC4 respectively), as computed by the following equation

$$F_{\max} = \left(\sum_n \mathbf{M}_{nC} \ \ddot{u}_n + \mathbf{M}_I \ddot{X} \right)_{\max} \tag{9}$$

		$F_{I,\max}$ [MN]	$F_{C,\max}$ [MN]
Tank1	*ACC1*	16.757	1.064
	ACC2	16.749	1.149
	ACC3	16.765	1.968
	ACC4	16.778	1.675
Tank2	*ACC1*	11.173	0.682
	ACC2	11.168	0.687
	ACC3	11.178	0.578
	ACC4	11.187	0.531
Tank3	*ACC1*	75.323	2.799
	ACC2	75.287	3.042
	ACC3	75.358	2.907
	ACC4	75.416	2.878

Table 1: Maximum impulsive and maximum convective force for 4 typical artificial seismic inputs (0.25g).

		$F_{C,\max} + F_{I,\max}$ [MN]	$\sqrt{\left(F_{C,\max}\right)^2 + \left(F_{I,\max}\right)^2}$ [MN]	$F_{\max}(t)$ [MN]
Tank1	*ACC1*	17.822	16.792	16.888
	ACC2	17.899	16.789	17.001
	ACC3	18.734	16.881	16.823
	ACC4	18.454	16.862	17.101
Tank2	*ACC1*	11.856	11.194	11.303
	ACC2	11.856	11.189	11.632
	ACC3	11.757	11.194	10.845
	ACC4	11.719	11.200	11.620
Tank3	*ACC1*	78.123	75.376	74.689
	ACC2	78.329	75.349	75.207
	ACC3	78.267	75.415	75.364
	ACC4	78.295	75.471	76.075

Table 2: Combination of maximum impulsive and maximum convective forces.

The values in Tables 1 and 2 indicate the following

- The impulsive force is significantly higher than the convective force. Therefore, in most of the cases, refinements on the value of the convective force are of little importance on the calculation of the total seismic force.
- In the special case, of broad tanks (low values of tank aspect ratio), consideration of more than one sloshing mode (e.g. two sloshing modes) may be necessary for determining of the total seismic force, due to the appropriate determination of impulsive mass M_I in equation (7), rather than the contribution of higher modes on the value of the maximum convective force F_C.
- The combination of impulsive and convective forces should be conducted according to the SRSS rule, rather than the addition of the maximum convective and maximum impulsive forces.

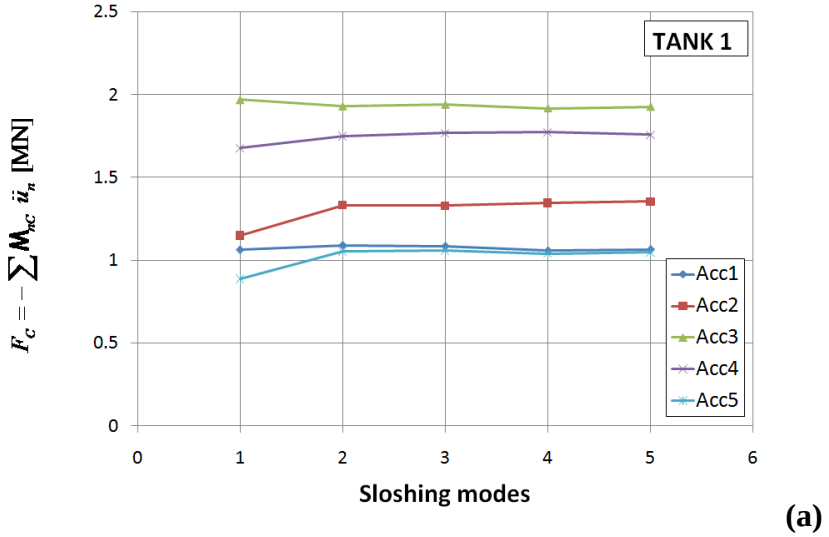

(a)

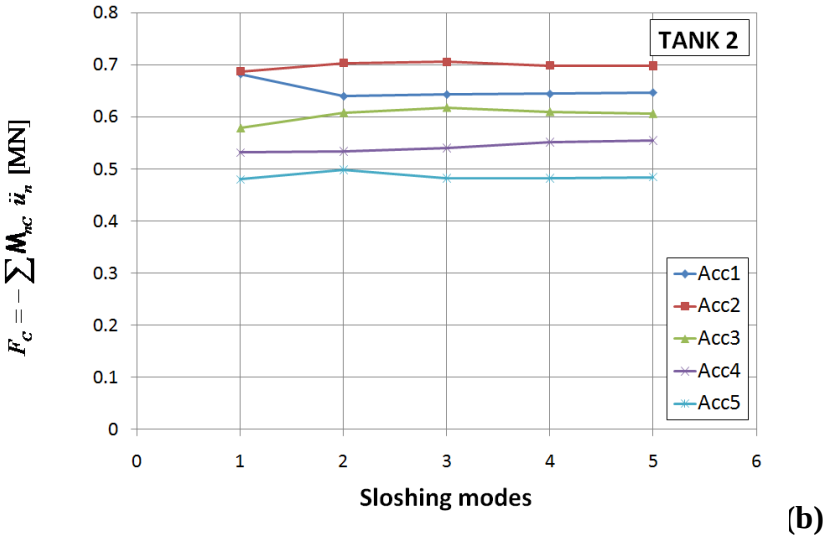

(b)

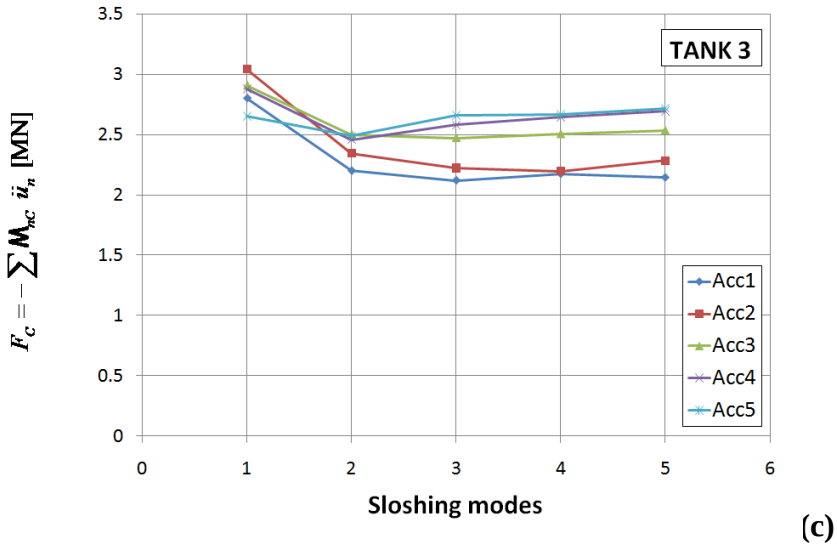

(c)

Figure 3: Effect of the number of sloshing (convective) modes on the maximum horizontal convective force for 5 typical ground acceleration excitations (a) Tank I; (b) Tank II and (c) Tank III.

4 EFFECTS OF TANK DEFORMABILITY

In the case of rigid (non-deformable) liquid containers, the impulsive motion is exactly the same as the ground motion, whereas the convective motion is determined by the solution of the hydrodynamic problem within the rigid container. However, steel tanks are not rigid, they deform due to their small thickness with respect to their diameter.

A finite element analysis, which accounted for the dynamic interaction between the liquid and the deformable tank, has been reported by Scharf [8]. Scharf's analysis it is assumed that in flexible tanks the motion of the tank-liquid system is expressed as the sum of three contributions, referred to as: 'rigid impulsive', 'sloshing' and 'flexible'. The third component of liquid motion satisfies the condition that the radial velocity of the fluid along the wall equals the deformation velocity of the tank wall, as well as the conditions of zero vertical velocity at the tank bottom and zero pressure at the free surface of the fluid. The total seismic force is given by the following expression

$$F = \mathbf{M}_I \ \ddot{u}_I + \sum_n \mathbf{M}_{nC} \ \ddot{u}_n + \mathbf{M}_f \ \ddot{a}_f \tag{10}$$

In the above expression, the deformation mass $\mathbf{M}_f$ is multiplied by the generalized coordinate $\ddot{a}_f$, which expresses the acceleration of the container relative to its base:

$$\ddot{a}_f + 2\xi_f \omega_f \dot{a}_f + \omega_f^2 a_f = -\ddot{X} \tag{11}$$

where ω_f is the natural frequency of the deformation motion. Due to the fact that the dynamic coupling between the sloshing and the flexible components is very weak, due to the large differences between the frequencies of the sloshing motion and of the deformation of the wall, which allows determining the third component of the motion (the deformation component) independently of the others. The rigid impulsive and the sloshing components for non-deformable tanks remains therefore unaffected [10]-[12]. In the work of Scharf [8], closed-form expressions for the impulsive frequency and the deformation mass are reported, and those expressions are included in section A.3.1 of the Informative Annex A of EN 1998-4, stated below:

$$\omega_f = 2\pi \frac{\sqrt{E\left(t_{1/3}\right)/\rho H}}{2R(0.157\gamma^2 + \gamma + 1.49)} \tag{12}$$

where $t_{1/3}$ is the thickness of the tank shell at height equal to $H/3$, and

$$\frac{\mathbf{M}_f}{\mathbf{M}_L} = \psi\gamma \sum_{n=0}^{\infty} \frac{(-1)^n}{\nu_n} d_n \tag{13}$$

where

$$d_n = 2 \frac{\left[\int_0^1 f(\zeta)\cos(\nu_n \zeta) d\zeta\right]}{\nu_n} \frac{I_1(\nu_n/\lambda)}{I_1'(\nu_n/\lambda)} \tag{14}$$

$\nu_n = (2n+1)\pi/2$, and ψ is a dimensionless parameter that depends on the shape function $f(\zeta)$ and is given by an awkward expression in EN 1998-4, paragraph A.3.1. Scharf [8] de-

scribes a tedious iterative methodology that results in the determination of shape function $f(\zeta)$.

In lieu of such a rigorous and tedious analysis described above, simplified models have also been developed to account for the interaction between the deformable cylindrical tank and the liquid. Such a model has been reported by Veletsos et al. [10], which constitutes the basis of the API 650 provisions [3] in calculating the impulsive seismic force. Similar to Scharf's formulation [8], the Veletsos' model [10] further assumes that the convective motion of the liquid remains unaffected by tank shell deformation. Therefore, the hydrodynamic solution for the rigid container is still applicable, and the tank shell deformation affects only the impulsive motion. This methodology has been adopted by the API 650 provisions, whereas the simplified methodology for deformable containers in section A.3.2.2 of EN 1998-4 is in-line with this approach. In particular, the latter provisions specify an impulsive frequency according to the equation (8), and the maximum seismic force is given by the following equation:

$$F = \mathbf{M}_I \ \ddot{u}_I + \sum_n \mathbf{M}_{nC} \ \ddot{u}_n \tag{15}$$

where the impulsive mass, the convective masses and the generalized coordinates u_I and u_n are given by equations (2) and (6) respectively. Assuming the same damping ratio for the impulsive and the deformation motion ($\xi_f = \xi_I$), one readily concludes that the two expressions (10) and (15) for the total seismic force provide identical results provided that (a) the two natural frequencies ω_f and ω_I are equal and (b) the corresponding masses $\mathbf{M}_f$ and $\mathbf{M}_I$ are equal.

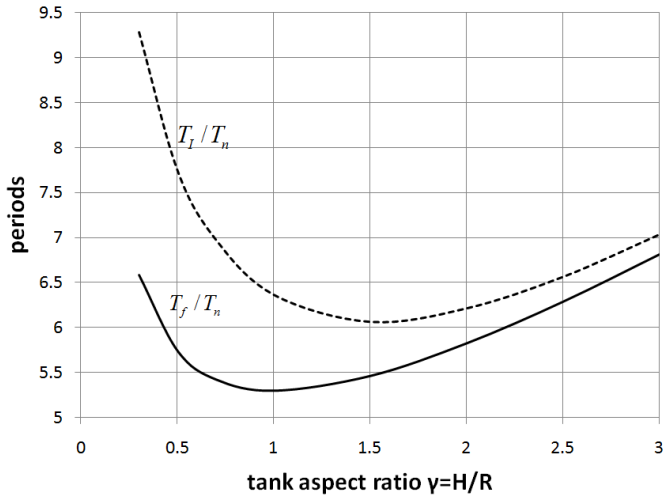

Figure 4: Comparison between the impulsive and the deformation natural periods (T_f and T_I).

The comparison between the impulsive and deformation frequencies is offered in Figure 4, in terms of the corresponding natural periods T_f and T_I, where both periods are normalized by the value of $T_n = \sqrt{\rho R H^2 / E t}$, so that $T_f^* = T_f / T_n$ and $T_I^* = T_I / T_n$, and assuming that the average thickness of the tank shell is equal to the value of $t_{1/3}$. The comparison of the two masses $\mathbf{M}_f$ and $\mathbf{M}_I$ is offered in Figure 5. The value of $\mathbf{M}_f$ is directly obtained by a similar

graph in [8]. In the same graph, points (1) and (2) refer to the value of M_f obtained through the application of equations (13) - (14) and assuming a shape function $f(\zeta)$ equal to ζ^2 and ζ respectively.

The above comparison indicates that there exist some differences between the two natural frequencies ω_f and ω_I, and the masses M_f and M_I. However, it is the authors opinion that the simplified methodology proposed by Veletsos et al. [10] can be used for the efficient calculation of seismic action on deformable liquid storage steel tanks.

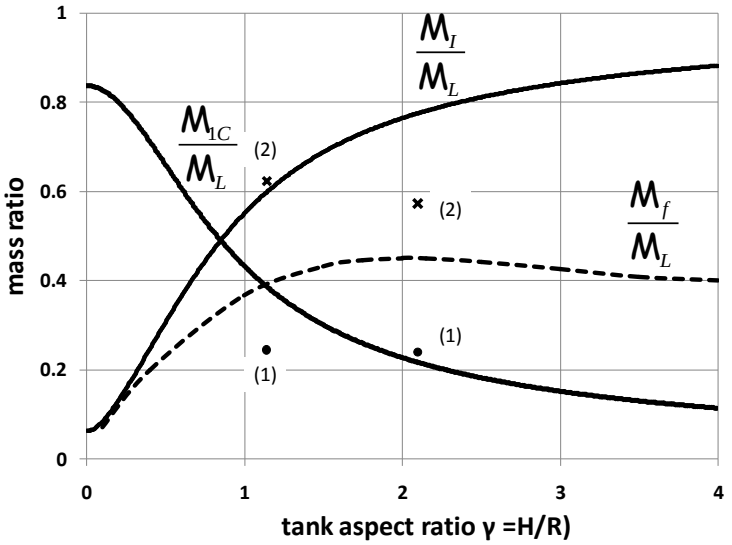

Figure 5: Comparison between the impulsive and the deformation masses (M_f and M_I).

5 CALCULATION OF HOOP HYDRODYNAMIC STRESSES

Thickness design of liquid storage tanks is based on hydrostatic pressure and the corresponding allowable stress of the tank material, as described in section E.6.1.4 of API 650. This calculation neglects the fact that during an earthquake event, additional hoop stresses will developed due to hydrodynamic loading, which need to be added to the stresses from the hydrostatic pressure and compared with the allowable stresses. A methodology for calculating hoop stresses has been proposed in the paper of Wozniak & Mitchell [13] based on the work of Veletsos [10], but up to 2007, it was not considered in design. For the first time, consideration of hoop hydrodynamic stresses and their superposition with the hydrostatic stresses is stated in the new Appendix E of API 650, 2007 edition [3]. On the other hand, there is no special provision of such a methodology in EN 1998-4 [6].

Explicit equations for computing hoop hydrodynamic stresses for the convective and impulsive component of liquid motion (denoted as σ_C and σ_I respectively) are stated in section E.6.1.4 of API 650 (not repeated herein for the sake of brevity), and should be superimposed with the hydrostatic pressure σ_h to obtain the total hoop stress σ_T in the course of seismic event as follows:

$$\sigma_T = \sigma_h \pm \sqrt{\sigma_I + \sigma_C} \tag{16}$$

The predictions of the above equation are compared with finite element results in Table 3, for the three tanks (Tanks I, II and III), which were described in section 1. Linear elastic analysis of the tanks is conducted, where the tanks are modeled with 4-node reduced-integration shell finite elements, and the hydrodynamic pressures (impulsive and convective) are applied on their lateral surface according to the following expressions. The impulsive pressure is

$$p_I(\zeta,\theta,t) = C_I(\zeta)\rho H \cos\theta \ddot{X} \tag{17}$$

where ρ is the density of the contained liquid, H is the height from the base to the free surface of the liquid, $\zeta = z/R$ is the nondimensional coordinate along the tank height, θ is the circumferential angle, and $C_I(\zeta)$ is a function that depends on the aspect ratio of the tank. The convective pressure is

$$p_C = \rho\psi_1 \cosh(\lambda_n\gamma\zeta) J_1(\lambda_n\xi)\cos\theta \ddot{u}_{1C} \tag{18}$$

where:

$$\psi_1 = \frac{2R}{(\lambda_1^2 - 1) J_1(\lambda_1)\cosh(\lambda_1\gamma)} \tag{19}$$

and $\lambda_1 = 1.841$, $\gamma = H/R$, J_1 is Bessel function of the first order, $\ddot{u}_{1C}$ is the acceleration corresponding to the first sloshing mode. The above impulsive and the convective pressure distributions are imposed in the finite element model through a load-user subroutine. For simplicity, the possibility of uplifting in Tanks I and III is excluded, so that all tanks are considered mechanically anchored. The numerical results indicate a good comparison between the numerical results and the above predictions. Given the fact that EN 1998-4 does not include a methodology for calculating hoop hydrodynamic stresses, the corresponding API 650 equations can be used for an efficient prediction of hydrodynamic effects on the total hoop stress of the tank.

	Type of load	Hoop stress from finite element analysis (MPa)	Hoop stress from API 650 (MPa)
Tank I D=27.4m H=15.7m	hydrostatic pressure	116	119
	hydrostatic pressure +earthquake	140	146.3
Tank II D=18m H=19m	hydrostatic pressure	167	168
	hydrostatic pressure +earthquake	190	200.3
Tank III D=68m H=19m	hydrostatic pressure	155	164
	hydrostatic pressure +earthquake	195	203.6

Table 3: Hoop hydrostatic and hydrodynamic stresses computed from finite element models and predicted by API 650.

6 UPLIFTING EFFECTS ON UNANCHORED TANKS

In most of practical applications, relatively broad liquid storage tanks are constructed unanchored, in the sense that their bottom plate is in simple contact with the ground, without anchor bolts. In such a case, under strong seismic loading, the tank may exhibit uplifting of its bottom plate, which may result in (a) excessive stresses at the connection between the bottom plate and the tank shell, and (b) increase of the maximum compressive stress at the shell bottom. This is shown schematically in Figure 6, referring to locations 1 and 2.

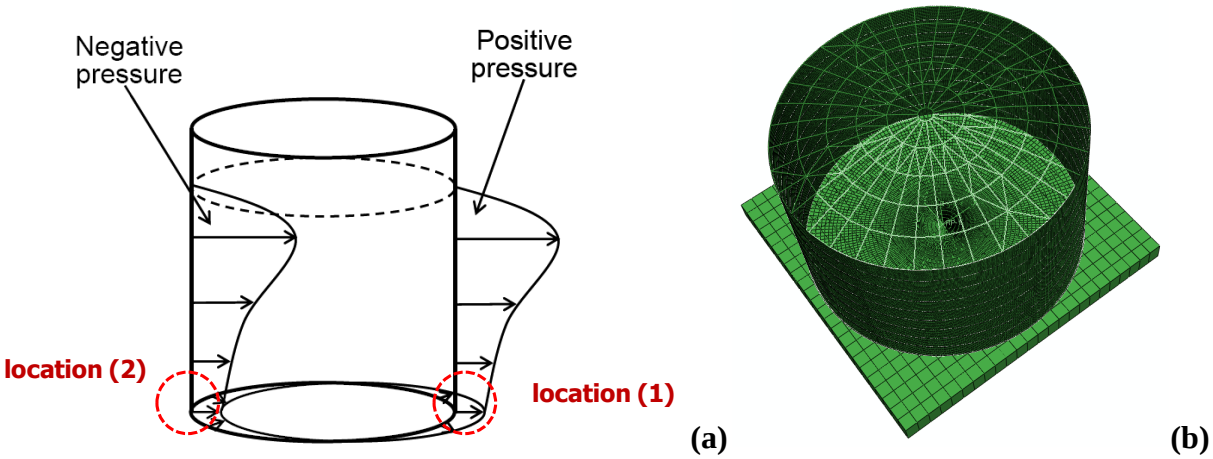

Figure 6: (a) Locations affected by uplifting during seismic action in an unanchored tank; (b) Numerical finite element model for uplifting analysis.

In current design practice, API 650 considers uplifting through the so-called anchorage ratio J defined as follows (neglecting the vertical component of seismic excitation, for the sake of simplicity):

$$J = \frac{M}{D^2\left[w_t + w_a\right]} \tag{20}$$

If the anchorage ratio is between the values of 0.785 and 1.54, the unanchored tank is stable but its base uplifts. The corresponding compressive stress at the tank shell bottom is given by following expressions, written in more convenient terms:

- For tanks without uplifting:

$$N_{anch} = w_t + \frac{1.273M}{D^2} \tag{21}$$

- For unanchored tanks with uplifting

$$N_{unanch} = \frac{w_t + w_a}{0.607 - 0.187\left(J\right)^{2.3}} - w_a \tag{22}$$

Paragraph A.9 of Annex A in EN 1998-4 standard describes a methodology for the uplifting effects of unanchored tanks, based on the work of Scharf [8], who conducted a finite element analysis of the tank-liquid system. These effects are presented in graphical form, where the increase of axial compressive stress due to uplifting is plotted against the overturning moment ratio M/WH .

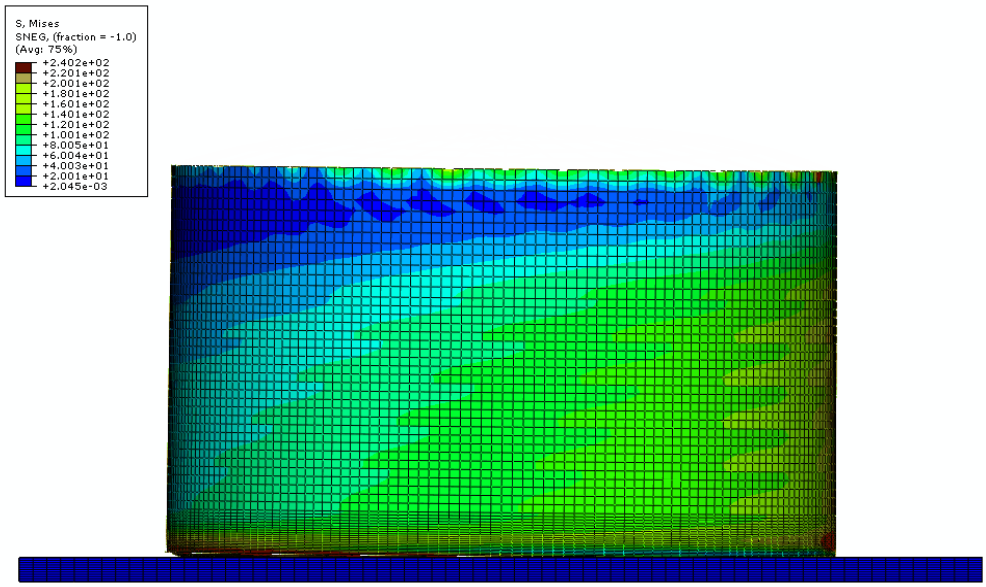

Figure 7: Finite element analysis of unanchored liquid storage tank under lateral loading.

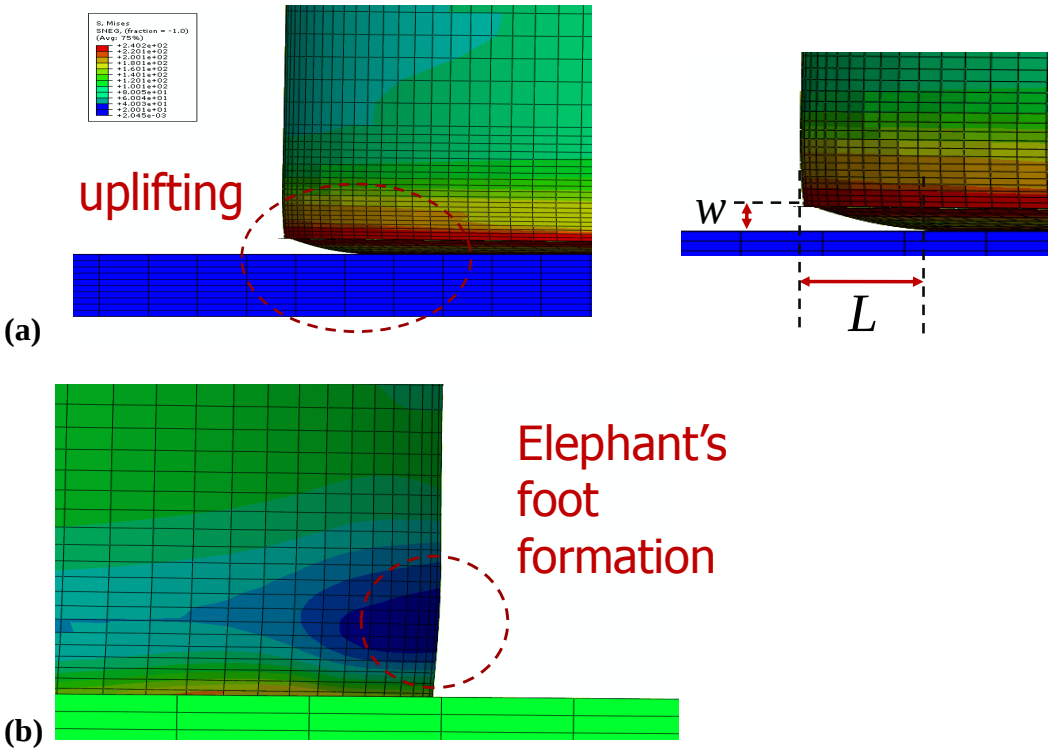

Figure 8: Finite element analysis of unanchored liquid storage tank under lateral loading; (a) uplifting of base plate, (b) development of elephant's foot at the tank bottom.

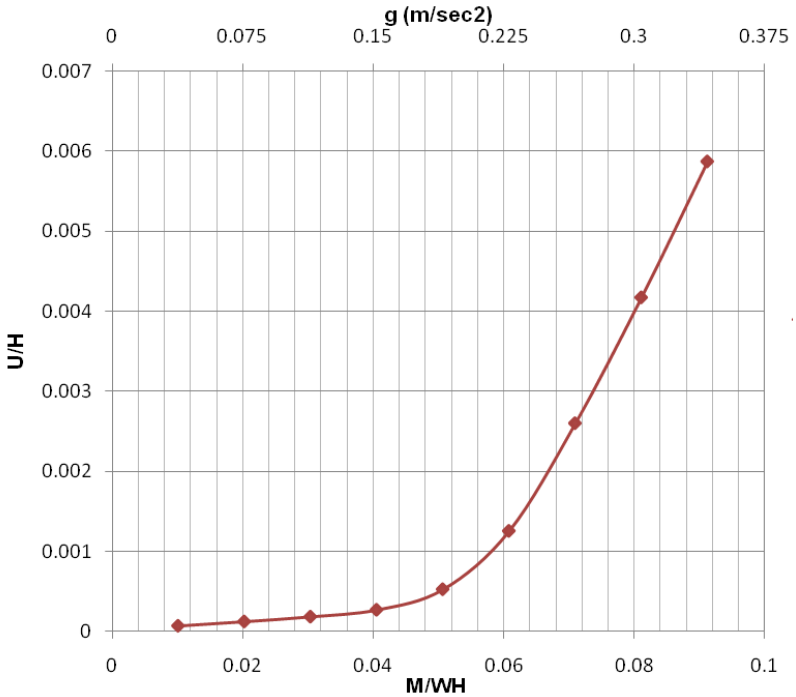

Figure 9: Overturning moment M versus top horizontal displacement U of tank, subjected to finite element pushover analysis.

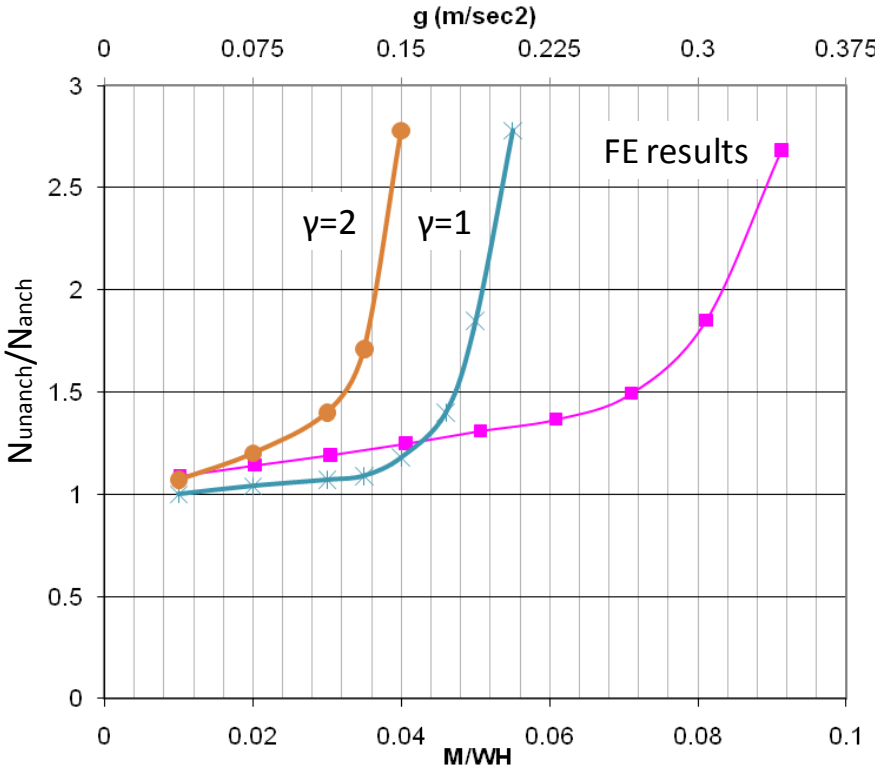

Figure 10: Increase of axial compressive stress on tank shell wall due to uplifting with respect to the overturning moment; finite element pushover analysis versus EN 1998-4 provisions.

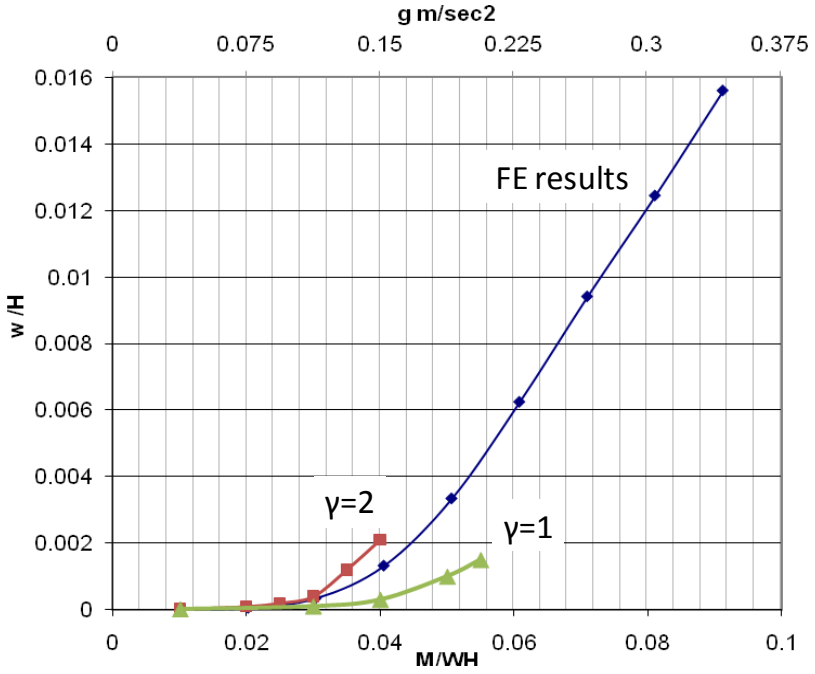

Figure 11: Uplifting size w in terms of overturning moment for Tank I; finite element pushover analysis.

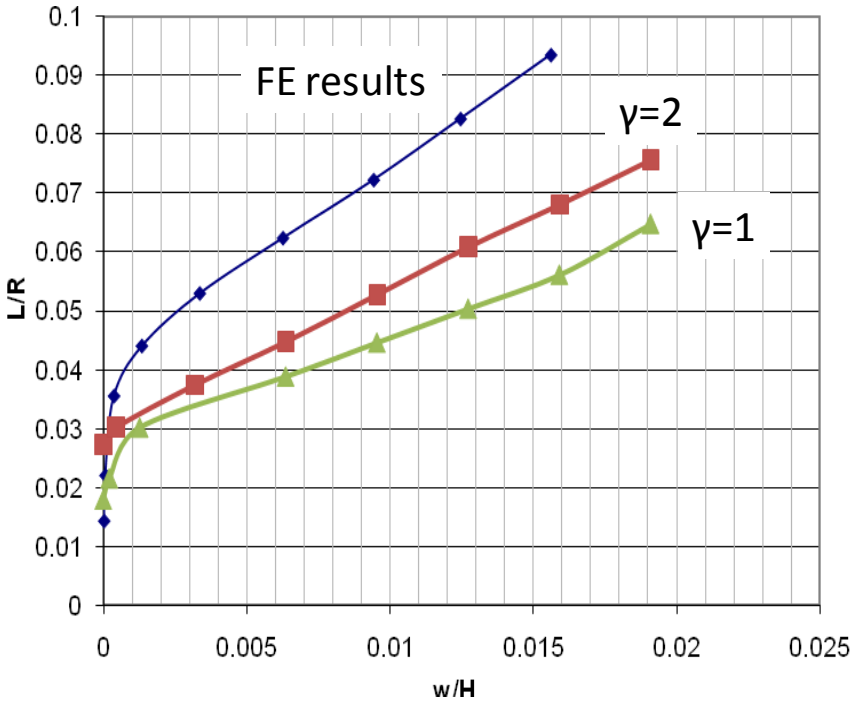

Figure 12: Uplifting length L in terms of uplifting size w for Tank I; finite element pushover analysis.

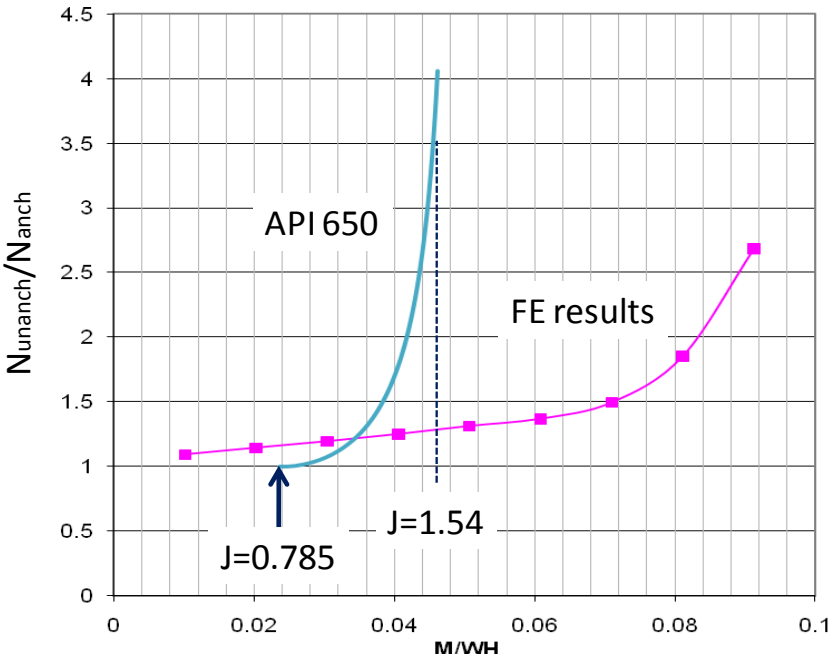

Figure 13: Increase of axial compressive stress on tank shell wall due to uplifting with respect to the overturning moment at the tank shell bottom; finite element pushover analysis versus API 650 provisions.

Herein, using more rigorous finite element simulation tools, the above API 650 and EN 1998-4 provisions for tank uplifting are evaluated. Special emphasis is given on effects of uplifting the compressive stress that causes elephant's foot buckling, which constitutes the major failure mode of the tank under strong earthquake loading. For this purpose, Tank I ($H/R=1.145$) was simulated with shell finite elements, with the model shown in Figure 6b. All parts of the interacting system were modeled: the tank shell, the truss roof, the base plate, the annular plate, and the ground. Four-node reduced-integration shell elements are employed to model the tank shell and the base/annular plates, the truss roof is modeled with beam elements, whereas solid elements are employed for modeling the ground. Contact conditions are considered between the base/annular plate and the ground, with friction coefficient equal to 0.3, allowing for tank uplift. The analysis is nonlinear static, and the hydrodynamic pressure is applied on the tank shell and the base plate for both the impulsive and the convective component. Considering this distribution of pressure, nonlinear "pushover" analysis is conducted controlling the value of the pressure multiplier, through a Riks continuation algorithm, which allows for the detection of possible instability (buckling) phenomena at the tank shell. Figure 7 and Figure 8 show the uplifting response of Tank I, as obtained by the present finite element simulation.

Figure 9 shows the horizontal displacement of the top of the tank in terms of the normalized overturning moment at the tank base M/WH. The value of M is obtained by an appropriate integration of the pressure on the tank shell surface. The increase of axial compressive stress due to uplift is shown in Figure 10 and the numerical results are compared with the graphs in EN 1998-4. The comparison shows that the EN 1998-4 curves are quite conservative in predicting the increase of axial stress due to uplift. In Figure 11 and Figure 12, the uplift magnitude and as the uplift length are plotted. Comparing the numerical results in Figure 9 and in Figure 11, one readily observes nonlinear inelastic behavior of the tank, as soon as some uplifting of the tank starts. This is associated with inelastic deformation at the uplifted

area of the base plate. Furthermore, the comparison between the numerical results and the curves of EN 1998-4 shows that the EN 1998-4 curves represent the general trend but are quite conservative in predicting the effect of uplifting on the axial compressive stress.

Finally, in Figure 13, the finite element results for the axial compressive stress increase due to uplifting are compared with the corresponding provisions of API 650, i.e. expressions (21) and (22). The comparison shows that the API 650 provisions are very conservative. However, this comparison is somewhat unfair, because the overturning moment in API 650 is calculated considering a large value of reduction factor. The value of the reduction factor is discussed in a subsequent section.

7 ELEPHANT'S FOOT BUCKLING

When subjected to earthquake loading, tanks may fail due to excessive compression at the bottom of the tank shell. This is a typical buckling mode of a thin-walled shell under the simultaneous action of meridional compression and hoop tension due to the presence of internal pressure, it is referred to as "elephant's foot buckling" and is considered as the major source of liquid storage tank failure under seismic action [14]. Figure 14 shows two characteristic cases of the elephant's foot buckling following strong earthquakes. In the following, elephant's foot is examined numerically, with emphasis on post-buckling strength.

The possibility of elephant's foot development in Tank I is examined, through the consideration of an axisymmetric finite element model. From Figure 14, it can be concluded that there is a quasi-uniform state of deformation along a significant part of the tank perimeter. Therefore, it is reasonable to assume axisymmetric conditions, for the simulation of this phenomenon, and a meridian strip of is modeled with axisymmetric shell finite elements, as shown in Figure 15. In particular, the tank area near its bottom is simulated (three bottom courses), and the compressive action is applied as external downward loading at the top of each subjected to compressive stresses. The annular plate and the base plate are modeled and frictionless contact is assumed between the plates and the foundation, allowing for uplifting.

Figure 14: Elephant's foot buckling caused by strong earthquake action.

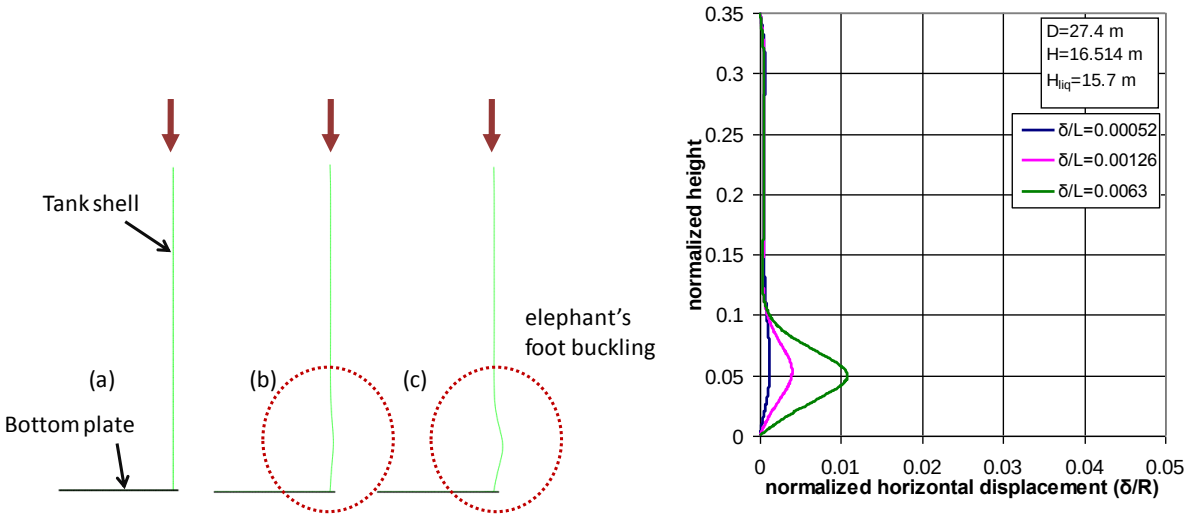

Figure 15: Development of elephant's foot, as predicted by the finite element analysis.

The results from the finite element analysis are shown in Figure 16, in terms of the equilibrium path of the applied axial stress on the tank wall in terms of the vertical and the horizontal outwards displacement of the tank wall. The most important observation refers to the fact that the The buckling shape obtained from the finite element analysis is shown in Figure 17 (in a three-dimensional form) and is very similar to observations from real earthquake events, as shown in Figure 14b. The most important observation refers to post-buckling response of the tank, which appears to be unstable; after reaching a maximum stress (load) the capacity drops very rapidly, indicating that the tank has not any ability of absorbing significant amounts of inelastic energy.

8 BUCKLING AT THE TOP OF THE TANK

Apart from elephant's foot buckling at the tank bottom, previous experience has indicated that liquid storage tanks suffer from buckling at their top. This is called "sloshing buckling" and it is shown in Figure 18. The first attempt to explain this phenomenon was report in the paper by Natsiavas and Babcock [15]. In that work, this type of buckling was attributed to the alternating sign of hydrodynamic (sloshing) pressure on the tank wall during the seismic excitation. More specifically, the tank under hydrostatic pressure exhibits tensile stresses on the tank shell that prevent buckling. However, when – in the course of a seismic event – this pressure becomes negative, i.e. directed inwards, it may overtake the internal (outward) hydrostatic pressure, so that the thin-walled tank top is locally under external pressure leading to shell buckling. It is important to note that, at the top of the tank, hydrostatic pressure is small, so that this overtaking is quite likely to occur, depending on the magnitude of the seismic action.

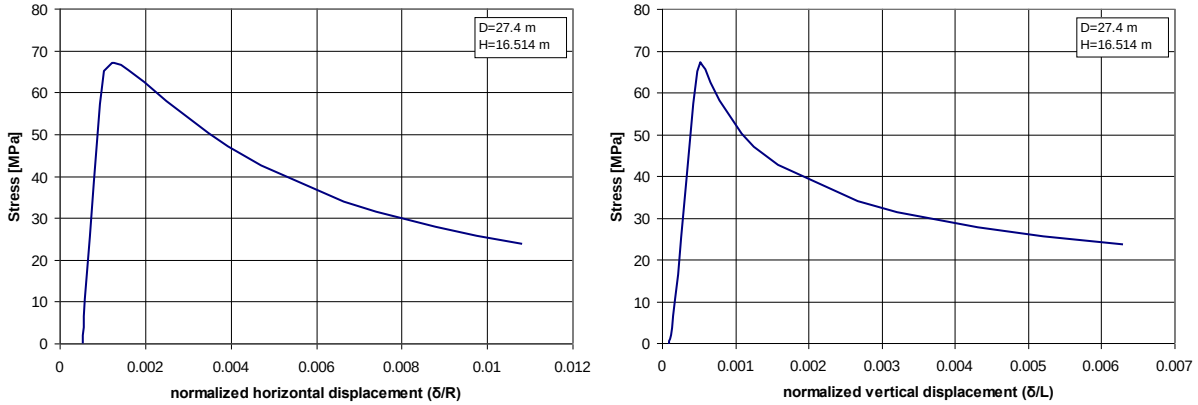

Figure 16: Compressive stress developed at the tank shell wall versus: (a) horizontal outward displacement of the wall, (b) vertical displacement at the top of the model.

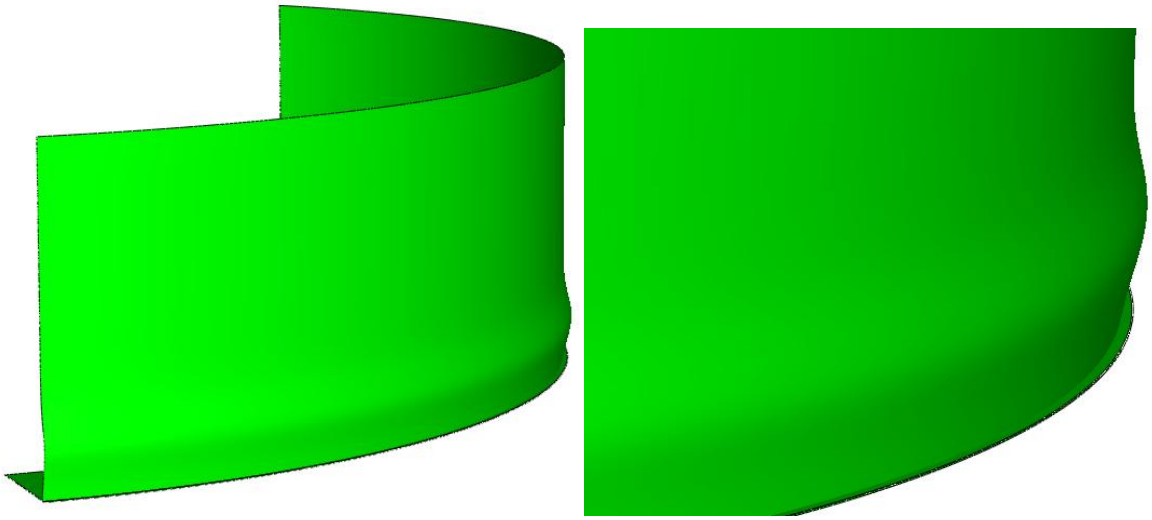

Figure 17: Elephant's foot buckling, as obtained by the finite element simulation.

To quantify this effect, Tank I is considered and the impulsive and convective pressures are computed at $\theta = 0$ and $\theta = \pi$ for 7 artificial earthquakes, corresponding to a maximum ground acceleration of 0.25g. Figure 19 shows the distribution of hydrostatic and hydrodynamic (maximum convective and maximum impulsive) pressure on the tank wall, at $\theta = 0$, for a typical earthquake. Considering that the hydrodynamic pressure are of alternating sign, the numerical results in this graph indicate that outward hydrodynamic pressures may become dominant at the top part of the tank, resulting in an external pressurization of the tank at those locations, leading to buckling. This is shown more precisely in Figure 20, where the hydrodynamic pressures are subtracted from the hydrostatic pressure. The graphs indicate that the external pressure of the tank shell extends over a significant part of its height d_C as shown in Table 4 for 10 earthquake inputs, corresponding to 0.25g.

Figure 18: Sloshing buckling at the top of a tank; Kocaeli, Turkey earthquake 1999 [1].

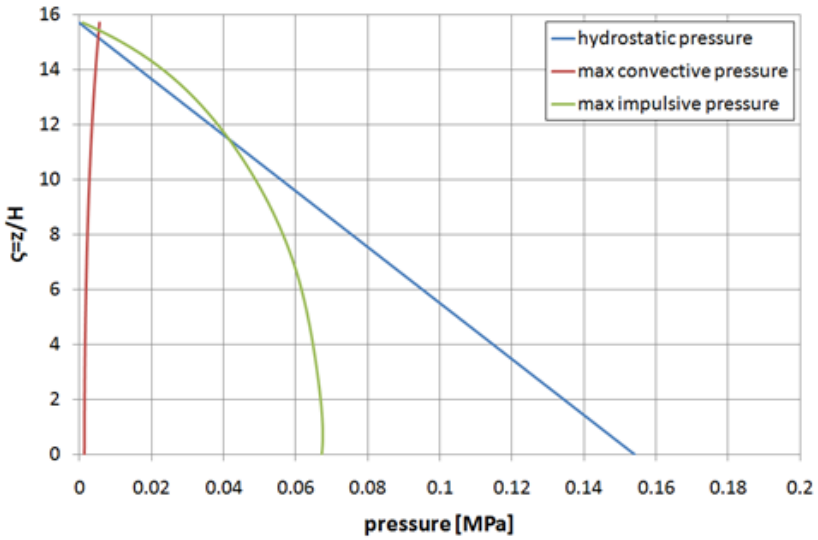

Figure 19: Distribution of hydrostatic pressure and maximum hydrodynamic pressures (impulsive and convective) along the height of Tank I for a characteristic seismic event of 0.25g.

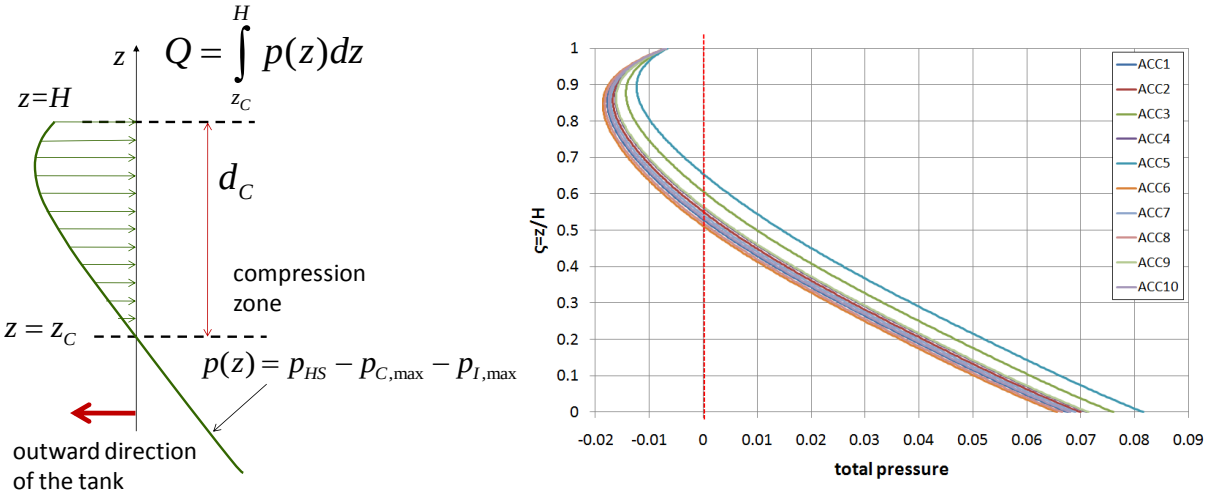

Figure 20: (a) Schematic representation of compressive (inward) pressures at the top of the tank; (b) Results from 10 artificial ground acceleration inputs (0.25g).

	Maximum impulsive acceleration [g]	**Maximum convective acceleration [g]**	**Height of compression zone d_C [m]**	**Force per unit circumferential length Q [kN/m]**
ACC1	0.790	0.05	7.40	89.35
ACC2	0.768	0.05	7.05	80.49
ACC3	0.711	0.05	6.15	60.51
ACC4	0.757	0.05	6.90	76.32
ACC5	0.660	0.05	5.40	46.05
ACC6	0.808	0.05	7.65	97.09
ACC7	0.777	0.05	7.20	84.04
ACC8	0.800	0.05	7.55	93.59
ACC9	0.754	0.05	6.85	75.20
ACC10	0.785	0.05	7.30	87.27

Table 4: Height of the compression zone at the top of the tank and corresponding inward force per unit circumferential length.

An estimate of the compressive hoop stress developed at the tank shell top can be obtained by considering the total inward force per unit circumference length Q distributed along the compression zone d_C (see Figure 20a), so that an equivalent external pressure is computed as follows

$$p_{eq} = f\frac{Q}{d_C} \tag{23}$$

where f is a factor accounting for the non-uniform distribution of pressure on the compression zone, From simple statics of thin-walled cylindrical shells, one can readily calculate the corresponding compressive hoop stress considering axisymmetric conditions around the location of maximum compression $\theta = 0$, one may assume that the top of the tank behaves as a circular under uniform external pressure and the corresponding compressive hoop stress is

$$\sigma_\theta = \frac{p_{eq}D}{2t} \tag{24}$$

Resistance of the thin-walled tank shell against this type of buckling is offered by considering one or more ring stiffeners at the top of the tank. The design of those ring stiffeners can be conducted according to the newly published ECCS European Design Recommendations for Shell Buckling [16]. It is the author's opinion that the stiffener dimensions should be increased to account for the nonlinear effects of liquid sloshing, as well as for the impulsive nature of the sloshing wave. Using the above analysis and considerations, the development of new specific rules for determining the buckling resistance of tank shell at its top is a necessity, but it is outside the scope of the present study.

9 A NOTE ON THE BEHAVIOR FACTOR FOR LIQUID STORAGE TANKS

The behavior factor to be used in the seismic design of liquid storage tanks has created quite some controversy. It is worth noticing that the API 650 provisions adopt totally different values than those of EN 1998-4, as shown in the following Table 5.

	Impulsive	Convective
API 650		
Self-anchored	3.5	2.0
Mechanically-anchored	4.0	2.0
EN 1998-4		
For all anchorage systems	1.5	1.0

Table 5: Values of behavior (reduction) factor for seismic design of liquid storage tanks.

A first observation refers to the smaller values for the convective motion in comparison with the impulsive motion. This is attributed to the fact that the convective response may not be capable at dissipating seismic energy. However, it is quite interesting to note that while EN 1998-4 specifies $q=1$ for the convective force, the API 650 rules specify $R=2$, which implies the presence of a dissipating mechanism in the convective (sloshing) motion.

Furthermore, there exist striking differences on the values of q and R for the impulsive component of the seismic force, which need some further investigation. The ductility of the structural system constitutes the main parameter for the reduction of the seismic force. In particular, considering elephant's foot buckling as the dominant mode of buckling, the numerical results presented in a previous section demonstrate the limited capability of the tank shell of absorbing and dissipating seismic energy due to their unstable post-buckling behavior. Communication of the authors with the API 650 drafting committee (see Acknowledgements below) indicated that the relatively high values of reduction factors R adopted by the American standards is based both on previous experience, as well as on other dissipation mechanisms such as radiation damping at the tank foundation (soil-tank interaction), the ductility of the anchor bolts, or the inelastic behavior of the base plate in the case of uplifted unanchored tanks. As far as elephant's foot buckling is concerned, the significant drop of strength following buckling, shown by the numerical results of Figure 16 are not in favor of using a value of behavior (reduction) factor significantly higher than unity. On the other hand, the moment-displacement curve of Figure 9, indicates that such a dissipating mechanism may exist in unanchored tanks exhibiting uplifting. In any case, the identification of appropriate seismic energy dissipation mechanisms that would allow the use of behavior factor larger than unity is an open research issue, which needs significant additional research effort.

10 NONLINEAR SLOSHING EFFECTS

The calculation of hydrodynamic forces described in the above sections was based on linear liquid hydrodynamic theory. The basic assumption for this theory is the small-amplitude of sloshing waves, allowing for the linearization of the liquid free-surface boundary condition. More specifically, assuming ideal fluid conditions, the liquid motion in a undeformed (rigid) container, under horizontal excitation displacement $X(t)$ in the x direction is described by the flow potential $\Phi(x,y,z,t)$, so that the liquid velocity is the gradient of Φ ($\mathbf{u}=\nabla\Phi$), which satisfies the Laplace equation in the liquid domain,

$$\nabla^2\Phi=\frac{\partial^2\Phi}{\partial x^2}+\frac{\partial^2\Phi}{\partial y^2}+\frac{\partial^2\Phi}{\partial z^2}=0 \tag{25}$$

subjected to the following boundary conditions at the wet surface of the vessel wall

$$\frac{\partial \Phi}{\partial n} = \dot{X}\left(\mathbf{e}_x \cdot \mathbf{n}\right) \tag{26}$$

In the free-surface, the liquid should satisfy the kinematic and the dynamic boundary conditions, shown below:

$$\frac{\partial \eta}{\partial t} + \frac{\partial \eta}{\partial x}\frac{\partial \Phi}{\partial x} - \frac{\partial \Phi}{\partial z} = 0 \tag{27}$$

and

$$\frac{\partial \Phi}{\partial t} + \frac{1}{2}\left(\nabla \Phi\right)^2 + g\eta = -\ddot{X}x \tag{28}$$

If small-amplitude sloshing is assumed, then keeping only the linear terms of η and Φ in the above equations, and eliminating η, one obtained the following combined condition, widely used for linear analysis:

$$\frac{\partial^2 \Phi}{\partial t^2} + g\frac{\partial \Phi}{\partial z} = 0 \tag{29}$$

The question is whether the assumption for small-amplitude sloshing is valid or not in the course of a strong earthquake. This requires an rigorous analysis based on either an asymptotic solution or a nonlinear finite element analysis of the liquid within the container, which is outside the scope of the present study. A preliminary analysis of this type has been conducted by Chen et al. [17], where the containment of rectangular liquid storage tanks have been modeled with finite elements through an in-house moving grid methodology, and subjected to several earthquake inputs. The results indicated that:

- Nonlinear effects may be non-important for the calculation of the total seismic forces
- In strong and distant (low-frequency) earthquakes, the liquid surface elevation (sloshing wave height) can be affected. For the majority of seismic events, this effect is not very important

The above preliminary results demonstrate that the use of linear sloshing theory for determining the seismic action on the tank wall adequate, verifying the expressions proposed in current design standards, whereas the possible nonlinear sloshing effects on the sloshing wave amplitude can be accounted for through an appropriate increase of freeboard height specified by the design specifications.

11 CONCLUSIONS

In this paper several issues on the dynamic behavior of liquid storage tanks have been addressed and investigated. The main conclusions can be stated as follows:

- For the majority of tanks, consideration of only one sloshing (convective) mode is adequate for the calculation of the total seismic force.
- The combination of the convective force with the impulsive force should be conducted according to the SRSS rule, which in accordance with the design provisions of API 650, Annex E.

- Numerical results show that the EN 1998-4 provisions provide a reasonable yet conservative of the increase of axial compression due to uplifting.
- A simple methodology is presented in order to design tanks against buckling at the top, due to liquid sloshing, using the concept of "equivalent" external pressure.
- The behavior (reduction) factor for the seismic design of liquid storage tanks is a controversial issue that has not been examined thoroughly so far. Because of the relatively low post-buckling strength of the shell tank, the authors would be quite cautious in using a behavior factor greater than 1.5 for the impulsive component of motion.
- Nonlinear sloshing effects on the seismic behavior have not been thoroughly investigated so far. Limited numerical investigations, reported elsewhere, indicated that their effects on the total seismic force may not be important, but they can have significant effects on freeboard considerations.

12 ACKOWLEDGEMENTS

This work was carried out with a financial grant from the Research Fund for Coal and Steel of the European Commission, within **INDUSE** project: "STRUCTURAL SAFETY OF INDUSTRIAL STEEL TANKS, PRESSURE VESSELS AND PIPING SYSTEMS UNDER SEISMIC LOADING", Grant No. RFSR-CT-2009-00022. The authors also wish to thank Dr. Steven W. Meier, TANK INDUSTRY CONSULTANTS, INC., member of the AWWA D100 and API 650 drafting committees, for his valuable comments on the reduction (behaviour) factor for tank seismic design.

REFERENCES

[1] Suzuki K. (2002), "Report on damage to industrial facilities in the 1999 Kocaeli earthquake, Turkey.", *Journal of Earthquake Engineering*, Vol. 6, No. 2, pp. 275-296.

[2] Nielsen R. and Kiremidjian A. (1986), "Damage to oil refineries from major earthquakes.", *ASCE Journal of Structural Engineering*, Vol. 112, No. 6, pp.1481-1491.

[3] American Petroleum Institute (2007), *Seismic Design of Storage Tanks - Appendix E, Welded Steel Tanks for Oil Storage*, API 650, 11th Edition, Washington, D.C.

[4] American Petroleum Institute (2003), *Seismic Design of Storage Tanks - Appendix E, Welded Steel Tanks for Oil Storage*, API 650, 10th Edition, Washington, D.C.

[5] American Society of Civil Engineers (2006), *Minimum Design Loads for Buildings and Other Structures*, ASCE 7-05, Reston, VA.

[6] Comité Européen de Normalization (2006), *Silos, tanks and pipelines, Eurocode 8, part 4*, CEN/TC 250, EN-1998-4, Brussels.

[7] Rammerstorfer, F. G., Fisher, F. D. and Scharf, K. (1990), "Storage Tanks Under Earthquake Loading", *ASME Applied Mechanics Reviews,* Vol. 43, No. 11, pp. 261-283.

[8] Scharf, K. (1990), "Beiträge zur Erfassung des Verhaltens von erdbebenerregten, oberirdischen Tankbauwerken", *Fortschritt-Berichte VDI, Reihe 4. Bauingenieurwesen*, Nr. 97, VDI Verlag, Düsseldorf,.

[9] Rotter, J. M. (1990), Local Inelastic Collapse of Pressurized Thin Cylindrical Steel Shells under Axial Compression, *ASCE Journal of Structural Engineering*, Vol. 116, No.7, pp. 1955-1970

[10] Veletsos, A. S. and Yang, J. Y. (1977), "Earthquake Response of Liquid Storage Tanks", *2nd ASCE Engineering Mechanics Conference*, Raleigh, NC, pp. 1-24

[11] Haroun, M. A. and Housner, G. W. (1981), "Seismic Design of Liquid Storage Tanks", *ASCE Journal of the Technical Councils*, Vol. 107, No. 1, pp. 191-207

[12] Fischer, F. D., Rammerstorfer, F. G. (1999), "A Refined Analysis of Sloshing Effects in Seismically Excited Tanks"; *International Journal of Pressure Vessels and Piping*, Vol. 76, pp. 693-709.

[13] Wozniak, R. S. and Mitchell, W. W. (1978), "Basis of seismic design provisions for welded steel oil storage tanks", *Advances in Storage Tank Design*, API 43rd mid-year meeting, Toronto, Canada.

[14] O'Rourke, M. J. and So, P. (2000), "Seismic Fragility Curves for On-Grade Steel Tanks." *Earthquake Spectra*, Vol. 16, No. 4, pp. 801-815.

[15] Natsiavas, S. and Babcock, C. D. (1987), "Buckling at the Top of a Fluid-Filled Tank During Base Excitation", *ASME Journal of Pressure Vessel Technology*, Vol. 109, No. 4, pp. 374-380.

[16] European Convention for Constructional Steelwork (2008), *Buckling of Steel Shells, European Design Recommendations*, 5th Edition, ECCS Publication No. 125, J. M. Rotter and H. Schmidt Eds., Brussels, Belgium.

[17] Chen W., Haroun M. A., and Liu F. (1996), "Large amplitude liquid sloshing in seismically excited tanks", *Earthquake Engineering & Structural Dynamics*, Vol. 25, No. 7, pp. 653-669.